PHYSICAL REVIEW B VOLUME 32, NUMBER 5 1 SEPTEMBER 1985

Crystal-field transitions in f-electron oxides

S. Kern
Department of Physics, Colorado State University, Fort Collins, Colorado 80523

C.-K. Loong and G. H. Lander
Intense Pulsed Neutron Source, Argonne National Laboratory, Argonne, Illinois 60439

(Received 29 April 1985)

Neutron inelastic scattering has been used to measure for the first time the ground- to excited-state crystal-field transitions in PrO_2 (130 meV), $BaPrO_3$ (255 meV), and UO_2 ($\sim$160 meV). Details of these neutron experiments using the epithermal neutrons from the Argonne National Laboratory spallation source are given. From the observed transitions the following values of $V_4 = A_4\langle r^4\rangle$ are deduced: PrO_2 (-66 meV), $BaPrO_3$ (119 meV), and UO_2 (-385 meV). Comparisons are made with V_4 values deduced for metallic systems and those determined by optical techniques for dilute lanthanides in transparent hosts. In the case of UO_2, two peaks are seen, one at 155 meV and the other at 172 meV. This structure exists both below and above the Néel temperature T_N (30.8 K) and is discussed in terms of mechanisms that might exist in UO_2. Several further neutron experiments are suggested now that energy transfers above $\sim$100 meV may be measured at small (i.e., $\lesssim 5$ Å^{-1}) values of the momentum transfer.

I. INTRODUCTION

The lanthanide and actinide oxides form a particularly interesting set of compounds that have been widely investigated. The electronic structures have been studied with optical and photoemission techniques.[1-3] More recently band calculations[4] have suggested that the f electrons participate in the bonding process, so that experiments that focus on the f-electron behavior are of particular interest. One key piece of information regarding the f electrons that is missing is the extent of the crystal-field potential in the oxides. These potentials are difficult to calculate reliably as the point-charge values have to be adjusted for overlap terms, covalency, and screening.

The crystal field lifts the degeneracy of the electronic f levels within a given J multiplet and can result in a nonmagnetic ground state. The energy differences between these electronic states can usually be probed by optical techniques, with two important exceptions. First, if the material possesses inversion symmetry at the cation site then electric dipole transitions are forbidden, although they can sometimes be observed coupled with vibronic transitions. Second, if the material is opaque, which is the case for these oxides, then electronic Raman scattering is very difficult. Neutron scattering provides an alternative for probing both the electronic and vibronic states and does not suffer from these two disadvantages. Unfortunately, the range of energy transfers that is accessible with neutrons is small, and has been traditionally limited to a few tens of meV. (We shall use meV throughout this paper for energy, 1 meV = 8.065 cm^{-1} = 0.2418 THz = 11.606 K.) This turns out to be well matched to crystal-field splittings in *metallic* systems, in which much of the potential is screened by the conduction electrons.[5] The advent of spallation neutron sources[6] with their copious supply of epithermal neutrons promises to close the gap between optical and neutron spectroscopy.

The present work concerns the observation of the transitions between crystal-field states in the oxides PrO_2, $BaPrO_3$, and UO_2. All these excitations exceed 100 meV. The experimental details are given in Sec. II and the analysis and discussion in Sec. III. We discuss the values of $A_4\langle r^4\rangle$ deduced and relate them to those found in other systems. A short report about the experiments on PrO_2 has been published previously.[7]

II. EXPERIMENTAL DETAILS

All experiments have been performed on the high-resolution medium-energy chopper spectrometer (HRMECS) at the Intense-Pulsed Neutron Source (IPNS) at Argonne National Laboratory. A schematic diagram of the instrument is shown in Fig. 1(a). A phased Fermi chopper produces pulses of monochromatic neutrons which are incident on the sample. The energy and momentum transfers are determined by neutron time-of-flight techniques in over 150 detectors.[8] The energy resolution, $\delta E/E_0$, in general, depends on the chopper in use and varies with energy transfer but is approximately 3—4 %. Incident energies of 350, 500, and 800 meV have been used for these experiments.

The samples were prepared by standard methods, examined by x rays to measure the lattice parameters [for PrO_2, a(cubic) = 5.392 Å; for $BaPrO_3$ the structure is orthorhombic, $a = 6.181$, $b = 6.214$, and $c = 8.722$ Å; for UO_2, a(cubic) = 5.470 Å] and search for additional phases, which were not found. Previous work[7] has shown that the PrO_2 sample, which is the most difficult to prepare, is very close to stoichiometry. Because of the relatively low neutron flux at IPNS very large samples have to be used if good resolution is required. In each case 100—120 g of polycrystalline material was contained in a flat-plate sam-

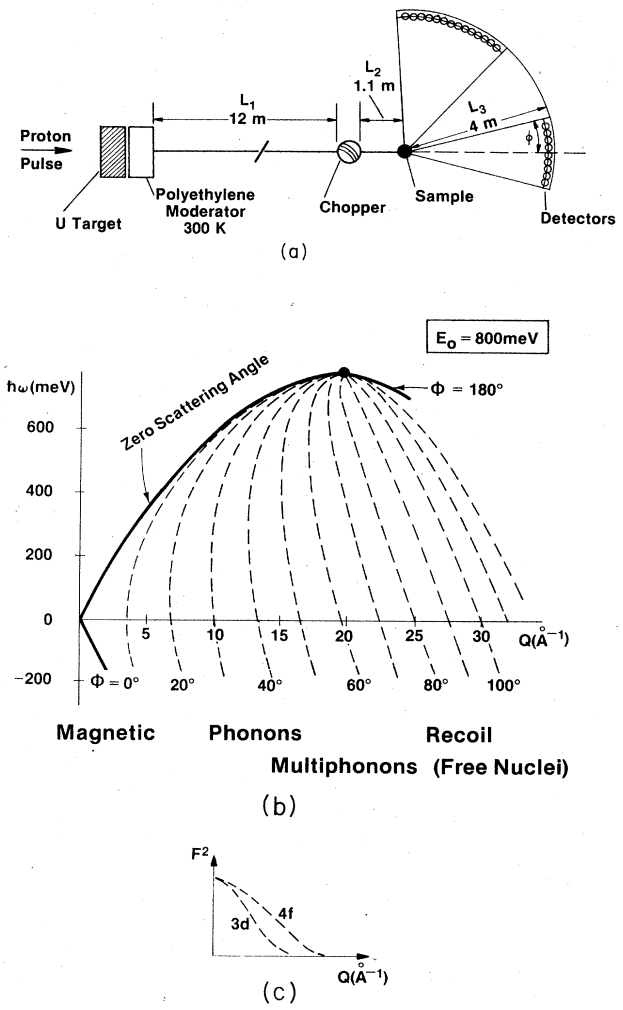

FIG. 1. (a) Schematic diagram of chopper spectrometer for neutron inelastic scattering at the Intense-Pulsed Neutron Source at ANL. The "white" neutron pulses emerging from the moderator are "chopped" so that monochromatic neutrons are incident on the sample. The source operates at 30 Hz and the chopper rotates at 270 Hz. The scattered neutrons are analyzed for the time of flight and scattered angle ϕ. (b) Loci of constant ϕ in (Q,ω) plane for an incident energy of 800 meV. Note that for $Q \lesssim 5$ Å^{-1} the scattering angles ϕ must be less than 20°. The dominant contributing mechanisms to the scattering for each region are indicated below the figure. (c) Square of the magnetic form factor plotted on the same Q scale as the center portion.

ple can and this holder was mounted on the cold plate of a DISPLEX refrigerator. The neutron beam (of dimensions 7.5×10.0 cm^2) was perpendicular to the plate so that for low angles the beam did not transverse more than 1 cm of material. Such a geometry minimizes multiple scattering of the neutrons. The high-angle (large-ϕ) part of the instrument was not available at the time of our experiments, and one important measurement on UO_2 was performed on the lower-resolution ($\delta E/E_0 \simeq 5\%$) chopper spectrometer. Samples of the nonmagnetic analogs CeO_2, $BaCeO_3$, and ThO_2 were also examined, but no crystal-field excitations were seen. Detector calibration and intensity normalization were provided by measurements of the elastic incoherent scattering from a thin plate of vanadium. Scattering from the empty Al sample containers was $<10\%$ of the total signal, and could be reliably subtracted.

The difficulties of neutron kinematics are particularly severe in these experiments. The neutron cross section is given by

$$\frac{d^2\sigma}{d\Omega\, d\omega} = N\left[\frac{1.91e^2}{2mc^2}g_J\right]^2 f^2(\mathbf{Q})\frac{k_f}{k_i} \times \sum \rho_n |\langle n|\mathbf{J}_\perp|m\rangle|^2 \delta((E_n-E_m)/\hbar-\omega)\,, \tag{1}$$

when $|n\rangle, |m\rangle$ are states belonging to a given J multiplet, $J_\perp$ is the component of the total angular momentum operator perpendicular to the scattering vector $\mathbf{Q}$, $\mathbf{k}_i$ and $\mathbf{k}_f$ are initial and final wave vectors of the neutron, respectively, ρ_n is the probability of state $|n\rangle$ being occupied and the energy difference between state $|n\rangle$ and $|m\rangle$ is $\Delta E = E_n - E_m$, $f(\mathbf{Q})$ is the magnetic form factor, and the other parameters have their usual meanings. In the neutron inelastic experiment both energy and momentum must be conserved; thus

$$\mathbf{Q} = \mathbf{k}_i - \mathbf{k}_f \tag{2}$$

and

$$\hbar\omega = \Delta E = \frac{\hbar^2}{2m}(k_i^2 - k_f^2)\,. \tag{3}$$

The first point to recall is that the experiments are performed with the neutrons losing energy. This is because crystal-field levels are populated by Boltzmann statistics so that for excited levels above ~ 50 meV ($=580$ K) the population of the states at 300 K is negligible. In fact, to reduce vibronic effects most neutron experiments are done well below room temperature. The second point is that because of a finite spatial extent of the magnetic f electrons, $f(Q)$ falls to a small value by $Q \sim 5$ Å^{-1}. The combination of these two factors means that very-high-incident-energy neutrons must be used and the scattering angles must be small. The so-called kinematic problem is illustrated in Fig. 1(b). Here an incident energy $E_0 = 800$ meV has been chosen. For the present experiments, depending on the ΔE required, we have used $E_0 = 350$, 500, or 800 meV. For magnetic scattering the form factor squared [Fig. 1(c)] dictates that $\phi \lesssim 20°$. At somewhat higher angles vibronic effects can be seen, and at even higher values of Q, the scattering approaches the single-particle limit with free nuclei scattering. In the present experiments we have seen no sharp peaks from vibronic effects because the Q values are small. However, a general background level of multiphonon scattering can be expected at all values of Q and adds greatly to the difficulty of determining the magnitude of diffuse magnetic

scattering.[9] Fortunately, in the present experiments we are searching for discrete peaks in the inelastic scattering.

The data for PrO_2 are already presented in Ref. 7, and we will not repeat them here. One peak is seen at (130±5) meV with a width of ~15 meV, which is slightly larger than ~10 meV resolution expected with $E_0=350$ meV. The results for $BaPrO_3$ are shown in Fig. 2. The transition here is at (255±10) meV, with a width of ~25 meV, which is the instrumental resolution with $E_0=800$ meV. The three spectra in Fig. 2 show that the peak intensity decreases with increasing scattering angle ϕ. This is because of the form factor, and the decrease in Fig. 2 is exactly as expected, showing unambiguously that the transition is magnetic in origin.

The data for UO_2 are shown in Fig. 3 as a function of temperature. We see in the case of UO_2 that two peaks are seen, particularly at low temperature, with a splitting between them of (17±2) meV. At low temperature the peaks are at (155±1) and (172±2) meV. The widths of the peaks are ~11 meV, which is essentially the expected resolution (~10 meV) with $E_0=350$ meV. We will discuss the detailed spectra of UO_2 below; for the purposes of the crystal-field splitting we note that the weighted mean of the two peaks is 160 meV. Figure 3 also shows a steadily rising background at lower energies. This signal is due to phonon scattering in UO_2. In fact, we find a wide maximum at ~45 meV, consistent with a reasonably high density of phonon states between 30 and 55 meV. Optical phonons extend up to almost 80 meV in UO_2.[10]

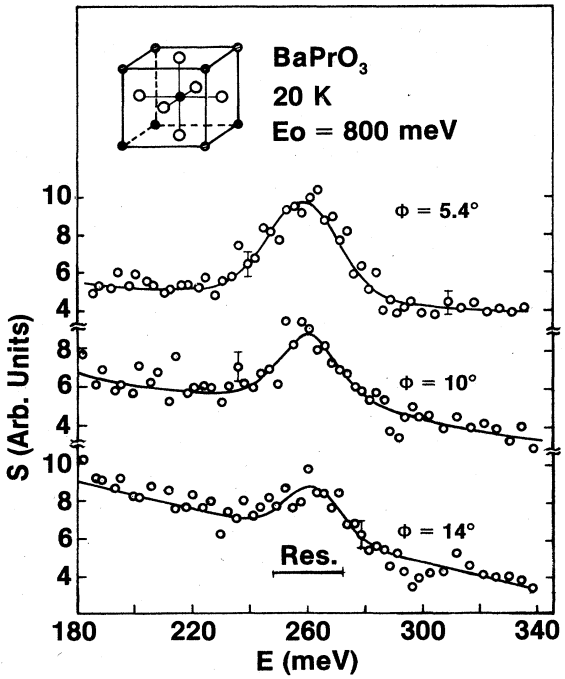

FIG. 2. Spectra for $BaPrO_3$ showing the Γ_7-Γ_8 splitting of 260 meV. The inset shows the octahedral coordination of the Pr ion. The frames of data at different ϕ have Q=3.9, 4.7, and 5.6 Å^{-1} from top to bottom, respectively, and show the decrease of intensity as expected from the magnetic form factor (see Fig. 1).

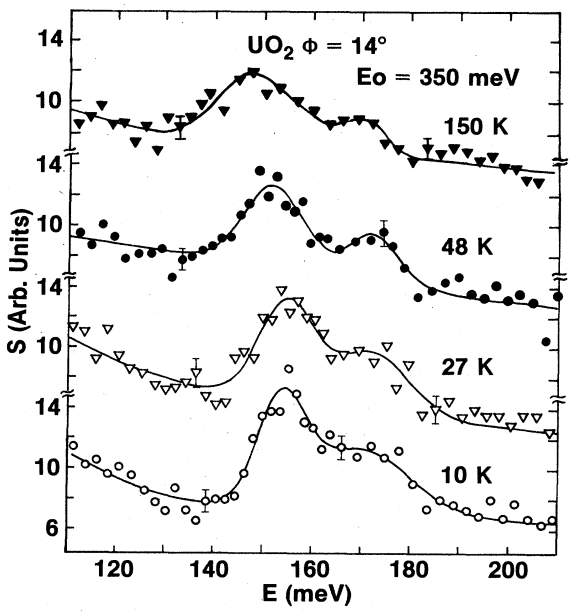

FIG. 3. Spectra for UO_2 as a function of temperature. The Q value at an energy transfer of 160 meV is 4.4 Å^{-1}.

III. ANALYSIS

A. Overall crystal-field parameters for Pr^{4+}

The general crystal-field Hamiltonian[11] for a cubic system may be written

$$H_{\mathrm{CEF}}=A_4\langle r^4\rangle\beta(O_4^0+5O_4^4)+A_6\langle r^6\rangle\gamma(O_6^0-21O_6^4)\ , \quad (4)$$

where β and γ are the Stevens factors, the O_l^m parameters are related to spherical harmonics, and the important parameters are $V_4=A_4\langle r^4\rangle$ and $V_6=A_6\langle r^6\rangle$, where $\langle r^n\rangle$ is the expectation value of the f electrons.

The ground-state multiplet for the Pr^{4+}:$4f^1$ configuration which is present in both PrO_2 and $BaPrO_3$ is $^2F_{5/2}$ with $J=\frac{5}{2}$ and $g=\frac{6}{7}$. The next J multiplet ($J=\frac{7}{2}$) is ~370 meV above the $J=\frac{5}{2}$ state. Complete calculations of the crystal-field states are illustrated in Fig. 4. Since we have observed only one transition in each case (the $\Gamma_8\rightarrow\Gamma_7$ in PrO_2, the $\Gamma_7\rightarrow\Gamma_8$ in $BaPrO_3$), we cannot determine the two parameters V_4 and V_6 independently for each material. Thus, we have made the reasonable assumption that $V_6/V_4\simeq 0.05$, and then calculated the V_4 necessary to give the observed splitting. Previously,[7] we obtained $V_4=-(57\pm3)$ meV for PrO_2. Considering the complete diagonalization and the small V_6 term, we now obtain $V_4=-(66\pm3)$ meV for PrO_2. For similar assumptions in $BaPrO_3$ we find $V_4=+(119\pm4)$ meV.

The relationship between these two values can also be estimated theoretically. In PrO_2 the configuration of the eight oxygens around the cation is cubic so that

$$V_4=A_4\langle r^4\rangle=-\frac{7}{18}\frac{Ze^2}{R^5}\langle r^4\rangle\ , \quad (5)$$

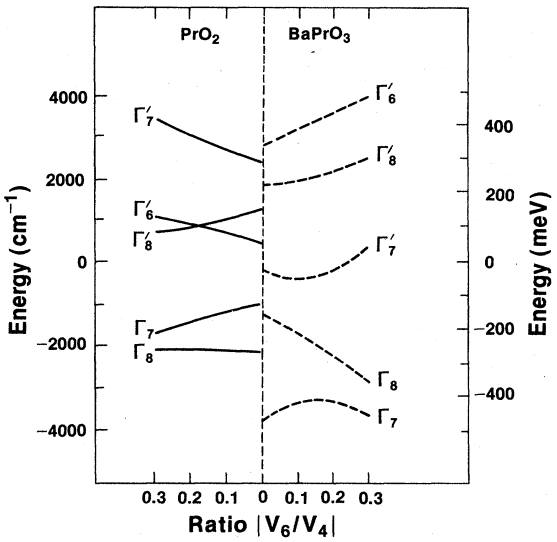

FIG. 4. Crystal-field diagram for Pr^{4+} in PrO_2 and $BaPrO_3$. The values of V_4 are -66 and 119 meV for PrO_2 and $BaPrO_3$, respectively. Excited states, with $J=\frac{7}{2}$ compared to the ground state with $J=\frac{5}{2}$, are indicated by primes. The experimental values are chosen to correspond to $V_6/V_4=0.05$ in each case.

where Ze is the effective charge at the ligand, and R is the rare-earth ligand separation. Higher-order terms from more distant neighbors have been neglected. The structure of $BaPrO_3$ is orthorhombic.[12] However, if we focus attention on the environment of the Pr^{4+} ion (see inset of Fig. 2) we find that the distribution of first-neighbor oxygen atoms is almost exactly octahedral. From Ref. 12 the two distances Pr-O are (2.23 ± 0.06) and (2.22 ± 0.03) Å. We assume an octahedral configuration in which

$$V_4=A_4\langle r^4\rangle=\frac{7}{16}\frac{Ze^2}{R^5}\langle r^4\rangle\ . \tag{6}$$

Thus, using the measured values of R, we would expect the ratio $V_4(PrO_2)/V_4(BaPrO_3)=-0.70$. Experimentally the value is $-(0.55\pm0.03)$. The calculated value of -0.70 is a consequence of the simple point-charge model with an R^{-n} behavior choosing $n=5$. In fact, there are numerous studies in the literature that point to a greater value for n, for example, Tovar, Ramos, and Fainstein,[13] give $n=9.7$ for Gd^{3+} in CaF_2. Considering the uncertainties in the distances in $BaPrO_3$ we find experimentally that $n=10\pm2$. This result is well within the calculated limits given by Axe and Burns[14] and used by Newman[15] in his superposition-model analysis of oxide materials. It is worth noting here that in metallic systems[16] the variation in crystal-field parameters, as well as the values themselves, obey the power law with $n=5$. Rather than confirm the validity of the simple point-charge model, this probably indicates that different screening mechanisms arise in the presence of conduction electrons.

B. Overall crystal-field parameters in UO_2

The crystal field and electronic ground state in UO_2 has been of considerable interest for the last two decades. The crystal-field scheme was first calculated in a classic paper by Rahman and Runciman.[17] Using complete diagonalization techniques, they calculated $V_4=-409$ meV, with a V_6/V_4 ratio of 0.06. The result of the calculation predicts a Γ_5 ground state, with Γ_3 as the first excited state separated by 170 meV from the ground state. This calculation has now been verified experimentally. We find the $\Gamma_5\rightarrow\Gamma_3$ splitting 160 meV (taking the weighted mean of the two peaks at low temperature) so that with $V_6/V_4\simeq0.06$, $V_4=-(385\pm10)$ meV. Note that we have assumed the Γ_5 is the ground state of UO_2, an assumption consistent with a great amount of experimental data, dating back to the infrared study by Allen,[18] the inelastic spin-wave measurements by Cowley and Dolling,[19] and the form-factor measurements of Faber and Lander.[20] We have plotted the crystal-field splittings for increasing V_4 for several values of V_6/V_4 in Fig. 5. Notice that there are several values of V_4, even ranges of values, for which the experimentally observed splitting of 160 meV is produced. Rahman and Runciman[17] used those values that gave a ground-state moment of $1.8\mu_B$, to match the magnitude measured by neutron diffraction below the Néel temperature and a ratio of V_6 to V_4 that seemed reasonable. If Allen's analysis[18] is correct then the moment projected out of crystal-field calculations must be close to the value of 2 μ_B observed if Jahn-Teller effects are to produce a reduced value of $1.8\mu_B$.

An important question remains as to whether the

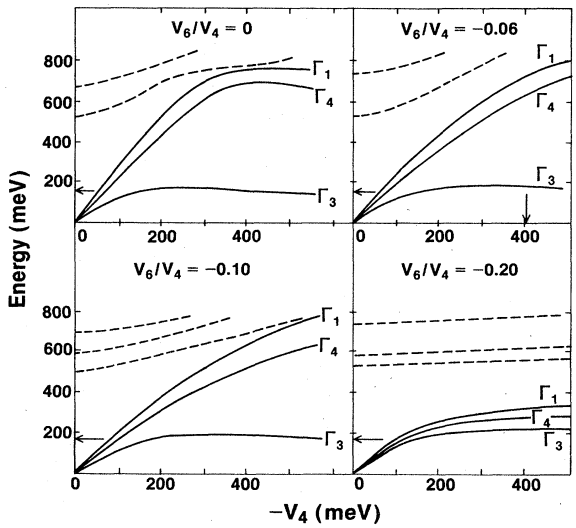

FIG. 5. Crystal-field diagram for UO_2. The Γ_5 ($^3H_4$) triplet is the ground state in each case and the calculation has been performed for various values of V_6/V_4 as marked. The solid lines correspond to those predominantly of $^3H_4$ representation and the dashed curves are schematic of the higher states below 800 meV. The arrow on the ordinate axes corresponds to the observation of 160 meV as experimentally observed (see Fig. 3). The arrow on the abscissa axis with $V_6/V_4=0.06$ indicates the predictions of Rahman and Runciman (Ref. 17).

second peak in Fig. 3 is not the $\Gamma_5 \rightarrow \Gamma_4$ transition. Indeed, if one follows the simple Russell-Saunders scheme adopted by, for example, Lea, Leask, and Wolf,[11] it is easily possible to obtain a close energy separation between the Γ_3 and Γ_4 excited states. We know that a more complete diagonalization is necessary and this we show for a variety of V_6/V_4 and V_4 values in Fig. 5. This figure shows clearly that for any reasonable value of $|V_6/V_4|$ (i.e., $\lesssim 0.10$) the Γ_3 and Γ_4 levels are separated by at least 100 meV. Thus it is unlikely that the second peak (at ~ 170 meV) in Fig. 3 arises from a $\Gamma_5 \rightarrow \Gamma_4$ transition. We can also examine the matrix elements for the $\Gamma_5 \rightarrow \Gamma_3$ and $\Gamma_5 \rightarrow \Gamma_4$ transitions. Within the $^3H_4$ ground state these are 4.0 and 3.5, respectively, with a ratio of 0.875 between them. If we take an extreme case of $V_4 = -200$ meV and $V_6/V_4 = -0.20$ (lower right-hand side of Fig. 5), then the admixture of higher S and L components in the intermediate-coupling wave function reduces this ratio to ~ 0.7. The observed ratio of the second peak at 170 meV to the first at 155 meV (Fig. 3) is close to 0.33, so this discrepancy also argues against the second peak arising from the $\Gamma_5 \rightarrow \Gamma_4$ transition. Experiments with $E_0 = 800$ meV on UO_2 have shown no other peaks in the region $200 < \Delta E < 350$ meV; thus the Γ_4 level is above 350 meV, again consistent with the assumption that $|V_6/V_4| \leq 0.10$.

We may now compare the values of V_4 for PrO_2 and UO_2. Using Eq. (5) we may deduce a value for Z_{eff}. Values of $\langle r^4 \rangle$ are needed, and we use 2.18 a.u. (Ref. 21) and 7.63 a.u. (Ref. 22) for Pr^{4+} and U^{4+}, respectively. For PrO_2, $Z_{\text{eff}} \simeq 4.8$, deduced from $V_4 = -66$ meV, and for UO_2, $Z_{\text{eff}} \simeq 8.6$, deduced from $V_4 = -385$ meV. The ratio of these values is consistent with the commonly accepted notion that the crystal fields in actinides are between 2 and 5 times stronger than those in the lanthanides because of the larger spatial extent of the $5f$ electrons.

C. Origin of double-peak structure in UO_2

The possibility that the second peak (at 172 meV) in UO_2 is caused by the $\Gamma_5 \rightarrow \Gamma_4$ transition is discussed above in connection with the calculations presented in Fig. 5 and found to be unlikely. We shall discuss below three other possibilities for this transition. First we affirm that *both* transitions are electronic in origin. We show in Fig. 6 data taken on the low-resolution ($\delta E/E_0 \sim 6\%$ at an energy transfer of 160 meV) medium-energy chopper spectrometer (LRMECS) at IPNS. From our earlier discussion magnetic scattering should decrease rapidly with increasing Q. In fact, from the form factor of UO_2 (Ref. 20) we expect

$$f^2(Q) \simeq \exp(-0.07Q^2)$$

for uranium $5f$ electrons. Scattering from electronic transitions should therefore be impossible to see for $Q \gtrsim 7$ Å^{-1}. In Fig. 6 we show data at Q values ranging from 3 to 19 Å^{-1} and the peak at ~ 160 meV, clearly disappears. Note that the resolution on LRMECS is not sufficient to separate the two peaks at 155 and 172 meV. Figure 6 definitely eliminates the possiblity that either transition is simply vibronic in origin, either from the UO_2 lattice itself or interstitial H for example. We note the following from Fig. 3. (i) The 172-meV peak is easily observable in the 10-, 27-, and 48-K data, but more difficult to see at 150 K. It is significant here that UO_2 orders antiferromagnetically at 30.8 K.[20] (ii) The main peak decreases in frequency by ~ 4 meV between 27 and 48 K. A further decrease of similar magnitude is observed as the material is warmed to 150 K. Some of this reduction is caused by the linear expansion of the lattice, thus changing R^{-n} in Eq. (5). In the case of UO_2 even with $n = 10$ the change in V_4 on warming from 10 to 300 K is about 2% (i.e., ~ 3 meV). Experimentally, we seem to observe something slightly greater than this.

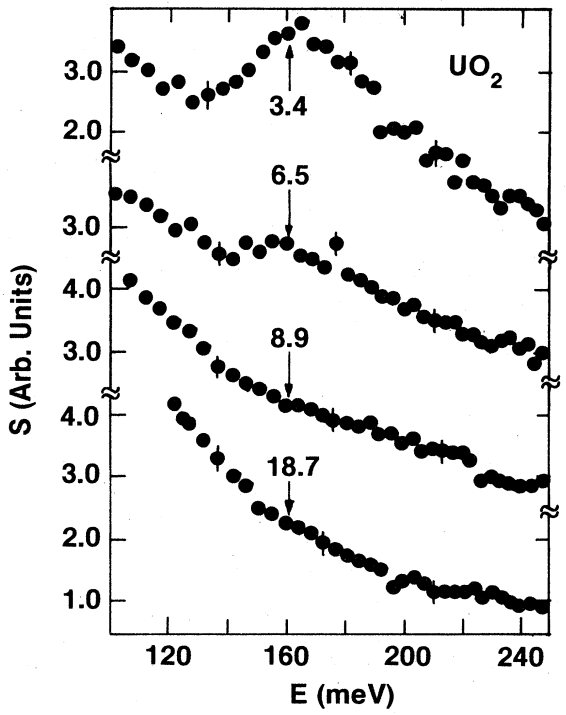

FIG. 6. Spectra of UO_2 at 10 K taken on the low-resolution chopper machine with $E_0 = 500$ meV. The Q values for an energy transfer of ~ 160 meV are marked on each spectrum.

(1) We believe a likely explanation for the double-peak structure in UO_2 at low temperature is a quadrupole interaction that lifts the degeneracy of excited Γ_3 doublet. It is known[20] that UO_2 distorts via an internal rearrangement of the oxygen sublattice, and this gives rise to additional terms in the crystal-field Hamiltonian, Eq. (4). In particular, terms in $A_2^0\langle r^2 \rangle$ are introduced ($A_2^2\langle r^2 \rangle$ is zero with the symmetry of this distortion in Ref. 20), as well as modifications to the ratio of $A_4^4\langle r^4 \rangle$ to $A_4^0\langle r^4 \rangle$, and $A_6^4\langle r^6 \rangle$. Given the *static* distortion of Ref. 20, in which the oxygen atoms move by 0.014 Å, we can calculate these additional terms. The largest change, that of

the ratio A_4^4/A_4^0, is $\sim 1\%$, compatible with the small static distortion. When these numbers are put into the crystal-field calculation, the Γ_3 level is split by ~ 2 meV, some 8 times smaller than the experimental observation. Despite this lack of agreement with the simplest of models, the quadrupole distortion in UO_2 is still a possibility. Sasaki and Obata[23] have shown that a *dynamical* Jahn-Teller effect in UO_2 has a pronounced effect on the susceptibility and extends to temperatures of ~ 200 K. Very large effects are also seen in the temperature dependence of the C_{44} elastic constants,[24] and these are not completely understood. A more recent search for phonon anomalies[25] yielded nothing unusual. We note that the increase in frequency (~ 4 meV) between 48 and 27 K, presumably at the ordering temperature, is probably due to the exchange splitting of the Γ_5 triplet. The spin-wave work[19] on UO_2 shows that the overall splitting of the Γ_5 triplet, as judged by the spin-wave frequency at the magnetic zone boundary, is ~ 13 meV. Although the dynamic Jahn-Teller effect in UO_2 is the most probable cause of the double peak, we anticipate sharp peaks below the Néel temperature T_N and a broad peak above T_N. This is not found experimentally.

(2) The second possibility is that a magnon-phonon interaction is giving rise to the double-peak structure. Again, as with (1) above, we should expect this to be pronounced below T_N, but small above it, which is not borne out experimentally. Strong magnon-phonon interactions are found in UO_2 at low energies,[19] but it is extremely difficult to formulate such interactions in a region where there are *no* phonon frequencies. A possibility is that double-phonon excitations are involved and we note here that Schoenes (see Fig. 18 of Ref. 3) observed a very sharp signal below T_N at 154 meV, which he identified as $2M$, in the phonon frequency. Raman scattering from ThO_2 shows several bands in this region. The Q dependence of our data argues strongly against a double-phonon interaction playing a role, but we cannot completely exclude it. The simplest phonon—crystal-field interaction as, for example, found in $CeAl_2$ requires the phonon and electronic excitations to be of comparable energy.[26]

(3) A third possibility is that the electronic f levels have dispersion in the Brillouin zone, and since in a polycrystalline material one essentially measures the density of states, one could assume that two major "bands" separated by ~ 17 meV are present. This dispersion must be in the Γ_3 doublet and cannot arise from simple exchange interactions since, again, it is present above T_N. However, dispersion in this energy range could be introduced by an interaction between the f and d states. Although the $5f^2 \rightarrow 6d(e_g)$ gap[3] is 3.05 eV, this does not preclude interaction effects that give rise to dispersion in $5f$-electronic states. An argument against this is that both peaks in Fig. 3 are essentially the same width (~ 11 meV) as the expected resolution. The dispersion must result therefore in two large, flat regions in the Brillouin zone, without any appreciable overlap. Although possible, this seems unlikely. Band-structure calculations[27] both show the f states well below E_F, and flat throughout the zone. However, the dispersion we require is very small—outside the resolution of present angle-resolved photoemission experiments. This effect, in contrast to (1) and (2) above, would be independent of the magnetic ordering, and thus more compatible with the experimental results. To examine such a hypothesis one would need to perform a neutron experiment on a single crystal of UO_2.

IV. SUMMARY

Experiments using the epithermal neutron spectrum of IPNS have, for the first time, allowed us to determine the ground- to excited-state crystal-field energies in a series of oxide materials. The limited beam intensities from IPNS, together with the severe kinematic restrictions (Fig. 1), do not presently allow us to extend these measurements beyond ~ 300 meV (~ 2400 cm^{-1}), so a complete characterization of *both* crystal-field parameters V_4 and V_6 is not possible. Instead, we have made the reasonable assumption that $V_6/V_4 \simeq 0.05$ and determined values for V_4.

We find consistency between the V_4 values for $Pr^{4+}(4f^1)$ in the cubic coordination in PrO_2 and the octahedral coordination in $BaPrO_3$, provided the nearest-neighbor interaction scales as R^{-n} with $n = 10 \pm 2$. This is in agreement with current models.[15]

The value of V_4 for UO_2 is not determined with any precision, because as Fig. 5 shows the Γ_5-Γ_3 splitting is not sensitive to the V_4 parameter provided that $V_4 \lesssim -200$ meV. Despite this limitation it is clear that the calculations of Rahman and Runciman[17] are a good approximation to the situation in UO_2 and that $V_4 \simeq -400$ meV. Comparison with PrO_2 indicates that the effective charge in UO_2 is about twice as great as in PrO_2, an expectation also in accord with models for lanthanide and actinide crystal fields. A more complete identification of the crystal-field parameters requires a more powerful spallation source, and possibly a different type of spectrometer. It is encouraging that a number of groups[6] are currently developing so-called eV spectrometers to measure energy transfers up to a few eV with small Q. The present materials, and perhaps UO_2 in particular, seem ideal candidates for such investigations.

Certainly the most interesting aspect of our measurements is the observation of a *doublet* for the $\Gamma_5 \rightarrow \Gamma_3$ transition in UO_2; see Fig. 3. Both transitions, at 155 and 172 meV, are electronic in origin. Since UO_2 orders antiferromagnetically at 30.8 K, the temperature independence of the doublet is most surprising. We know from earlier work that[18,19] below T_N there are very strong magnetoelastic effects in UO_2, and even small internal rearrangement of the oxygen atoms.[20] However, a quadrupole splitting of the Γ_3 state based on the lattice distortion of nearest-neighbor oxygen atoms gives a splitting much smaller (by almost a factor of 8) than experimentally observed. Moreover, this should disappear at T_N when the first-order antiferromagnetic-paramagnetic transition occurs. Instead, we believe that the effect is brought about by dynamic effects that also give rise to the anomalous behavior of the elastic constants.[24] A reexamination of the theory of Sasaki and Obata[23] with respect to the crystal-field energies and symmetries might allow a

better understanding of whether we could expect a resolved doublet for the $\Gamma_5 \rightarrow \Gamma_3$ transition. Two other possible explanations for this doublet structure are mentioned in Sec. III. Single-crystal experiments with UO_2 might also give further information on why this effect exists, and we plan such experiments at IPNS.

ACKNOWLEDGMENTS

IPNS is supported by the U.S. Dept. of Energy, Basic Energy Sciences, Division of Materials Science. One of us (S.K.) would like to thank the Institute for Computational Studies of Colorado State University for computer time granted on the CDC CYBER 205.

[1] *Handbook on the Physics and Chemistry of Rare-Earths,* edited by K. Gschneider and L. Eyring (North-Holland, Amsterdam, 1979), Chaps. 27 and 28.

[2] J. Schoenes, in *Handbook of the Physics and Chemistry of the Actinides,* edited by A. J. Freeman and G. H. Lander (North-Holland, Amsterdam, 1984), pp. 341–413.

[3] J. Schoenes, Phys. Rep. **63**, 301 (1980).

[4] D. D. Koelling, A. M. Boring, and J. H. Wood, Solid State Commun. **47**, 227 (1983); D. E. Ellis, V. A. Gubanov, and A. Rosen, J. Phys. (Paris) Colloq. **40**, C4-187 (1979).

[5] *Crystalline Electric Field Effects in f Electron Magnetism,* edited by R. P. Guertin, W. Suski, and Z. Zolnierek (Plenum, New York, 1982); see also Chap. 17 of Ref. 1.

[6] J. M. Carpenter, G. H. Lander, and C. G. Windsor, Rev. Sci. Instrum. **55**, 1019 (1984).

[7] S. Kern, C.-K. Loong, J. Faber, and G. H. Lander, Solid State Commun. **49**, 295 (1984).

[8] D. L. Price, J. M. Carpenter, C. A. Pelizzari, S. K. Sinha, I. Bresof, and G. E. Ostrowski, in Proceedings of ICANS-VI Conference 1982, ANL Report No. 8280 (unpublished), pp. 207–216 (ICANS denotes International Collaboration on Advanced Neutron Sources).

[9] M. Loewenhaupt, Physica **130B**, 347 (1985).

[10] G. Dolling, R.A. Cowley, and D. B. Woods, Can. J. Phys. **43**, 1397 (1965).

[11] K. R. Lea, M. J. M. Leask, and W. P. Wolf, J. Phys. Chem. Solids **23**, 1381 (1962).

[12] A. J. Jacobson, B. C. Tofield, and B. E. F. Fender, Acta Crystallogr. Sect. B **28**, 956 (1972).

[13] M. Tovar, C. A. Ramos, and C. Fainstein, Phys. Rev. B **28**, 4813 (1983).

[14] J. D. Axe and G. Burns, Phys. Rev. **152**, 331 (1966); G. Burns and J. D. Axe, in *Optical Properties of Ions in Crystals,* edited by H. M. Crosswhite and H. W. Moos (Interscience, New York, 1967).

[15] D. J. Newman, Adv. Phys. **20**, 197 (1971).

[16] R. J. Birgeneau, E. Bucher, J. P. Maita, L. Passell, and K. C. Turberfield, Phys. Rev. B **8**, 5345 (1973).

[17] H. U. Rahman and W. A. Runciman, J. Phys. Chem. Solids **27**, 1833 (1966).

[18] S. J. Allen, Phys. Rev. **166**, 530 (1968); **167**, 492 (1968).

[19] R. A. Cowley and G. Dolling, Phys. Rev. **167**, 464 (1968).

[20] J. Faber and G. H. Lander, Phys. Rev. B **14**, 1151 (1976); **13**, 1177 (1976).

[21] S. Kern and B. P. Das (unpublished).

[22] J. P. Desclaux and A. J. Freeman, J. Magn. Magn. Mater. **8**, 119 (1978).

[23] K. Sasaki and Y. Obata, J. Phys. Soc. Jpn. **28**, 1157 (1970).

[24] O. G. Brandt and C. T. Walker, Phys. Rev. **170**, 528 (1968).

[25] W. J. L. Buyers, T. M. Holden, G. Dolling, E. C. Svensson, and G. H. Lander, in *Proceedings of the 2nd International Conference on the Electronic Structure of Actinides,* edited by J. Mulak, W. Suski, and R. Troc (Polish Academy of Sciences, Warsaw, 1977), p. 395.

[26] P. Thalmeier, J. Phys. C **17**, 4153 (1984).

[27] P. J. Kelly and M. S. S. Brooks, J. Phys. C **13**, L939 (1980).